Inorganic Chemistry

Article

pubs.acs.org/IC

Combined Mössbauer Spectral and Density Functional Study of an Eight-Coordinate Iron(II) Complex

Gary J. Long* and Fernande Grandjean

Department of Chemistry, Missouri University of Science and Technology, University of Missouri, Rolla, Missouri 65409-0010, United States

Todd C. Harrop

Department of Chemistry, The University of Georgia, Athens, Georgia 30602, United States

Heather M. Petroccia and Georgia C. Papaefthymiou

Department of Physics, Villanova University, Villanova, Pennsylvania 19085, United States

Supporting Information

ABSTRACT: The iron-57 Mössbauer spectra of the eight-coordinate complex, $[Fe(L_{N4})_2](BF_4)_2$, where L_{N4} is the tetradentate $N^1(E),N^2(E)$-*bis*[(1-methyl-1H-imidazol-2-yl)methylene]-1,2-benzenediimine ligand, have been measured between 4.2 and 295 K and fit with a quadrupole doublet. The fit at 4.2 K yields an isomer shift, δ_{Fe}, of 1.260(1) mm/s and a quadrupole splitting, ΔE_Q, of 3.854(2) mm/s, values that are typical of a high-spin iron(II) complex. The temperature dependence of the isomer shift yields a Mössbauer temperature, Θ_M, of 319(27) K and the temperature dependence of the logarithm of the Mössbauer spectral absorption area yields a Debye temperature, Θ_D, of 131(6) K, values that are indicative of high-spin iron(II). Nonrelativistic single point density functional calculations with the B3LYP functional, the full 6-311++G(d,p) basis set, and the known X-ray structures for $[Mn(L_{N4})_2]^{2+}$, $[Mn(L_{N4})_2](ClO_4)_2$, **1**, $[Fe(L_{N4})_2]^{2+}$, and $[Fe(L_{N4})_2](BF_4)_2$, **2**, yield small electric field gradients for the manganese(II) complexes and electric field gradients and s-electron densities at the iron-57 nuclide that are in good to excellent agreement with the Mössbauer spectral parameters. The structure of **2** with a distorted square-antiprism C_1 iron(II) coordination symmetry exhibits four different $Fe-N_{imid}$ bonds to the imidazole nitrogens with an average bond distance of 2.253(2) Å and four different $Fe-N_{imine}$ bonds to the benzenediimine nitrogens, with an average bond distance of 2.432(2) Å; this large difference yields the large observed ΔE_Q. An optimization of the $[Fe(L_{N4})_2]^{2+}$ structure leads to a highly symmetric eight-coordination environment with S_4 symmetry and four equivalent $Fe-N_{imid}$ bond distances of 2.301(2) Å and four equivalent $Fe-N_{imine}$ bond distances of 2.487(2) Å. In contrast, an optimization of the $[Mn(L_{N4})_2]^{2+}$ structure leads to an eight-coordination manganese(II) environment with D_{2d} symmetry and four equivalent $Mn-N_{imid}$ bond distances of 2.350(3) Å and four equivalent $Mn-N_{imine}$ bond distances of 2.565(3) Å.

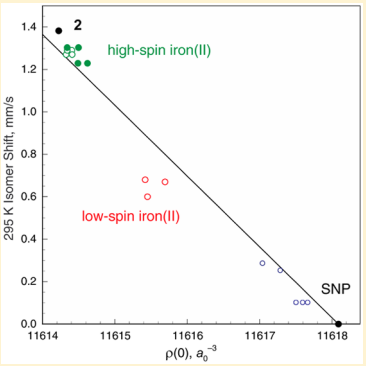

INTRODUCTION

Because eight-coordination is rather unusual for first-row divalent transition metal complexes, a detailed experimental and theoretical study of their electronic properties is important. Rather recently the single-crystal X-ray structures of the eight-coordinate manganese(II) complex, $[Mn(L_{N4})_2](ClO_4)_2$, **1**, and the iron(II) complex, $[Fe(L_{N4})_2](BF_4)_2$, **2**, where L_{N4} is the tetradentate ligand, $N^1(E),N^2(E)$-*bis*[(1-methyl-1H-imidazol-2-yl)methylene]-1,2-benzenediimine, see Scheme 1, have been reported.[1,2] These complexes provide a basis for the study of the electronic properties of two similar eight-coordinate complexes.

There are, of course, several papers[3−9] dealing either with eight-coordinate iron(II) complexes and/or with density functional calculations of their electronic properties that will be referred to and discussed below in relation to the results reported herein. Quite recently Conradie et al.[10] have used density functional calculations with several different functionals to determine both the relative energies of the frontier orbitals and the optimized structures of **1** and **2**. However, these authors did not report, for either the X-ray structure[2] of **2** or for its optimized structure, any calculated electric field gradients or s-electron densities at the iron(II) nucleus, two quantities that can be experimentally determined by Mössbauer spectroscopy.

Herein we report the 4.2 to 295 K temperature dependence of the Mössbauer spectra of $[Fe(L_{N4})_2](BF_4)_2$, **2** and use density functional calculations on both $[Fe(L_{N4})_2](BF_4)_2$, **2**,

Received: May 18, 2015
Published: August 12, 2015

DOI: 10.1021/acs.inorgchem.5b01121
Inorg. Chem. 2015, 54, 8415−8422

Scheme 1. Structure of the Dication in $[Fe(L_{N4})_2](BF_4)_2$, 2

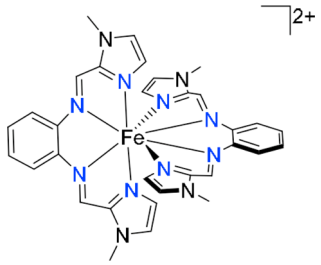

and $[Mn(L_{N4})_2](ClO_4)_2$, **1**, to better understand their electronic properties through the calculation of the electric field gradients and s-electron densities at the metal nuclei of the iron(II) and manganese(II) cations in these two eight-coordinate complexes.

EXPERIMENTAL METHODS

The syntheses of $[Mn(L_{N4})_2](ClO_4)_2$, **1**, and $[Fe(L_{N4})_2](BF_4)_2$, **2**, have been reported[1,2] earlier; the same sample of **2** as was studied earlier has been used for the Mössbauer spectral studies reported herein.

The iron-57 transmission Mössbauer spectra have been obtained on a polycrystalline sample of **2** dispersed in boron nitride by using a conventional constant acceleration Mössbauer spectrometer that was equipped with a rhodium based cobalt-57 source and was calibrated at 295 K with an iron-57 enriched α-iron foil. The isomer shifts are reported relative to α-iron as δ_{Fe}; the corresponding values are given relative to sodium nitroprusside, SNP, as δ_{SNP} by adding 0.2649(8) mm/s to δ_{Fe}. The temperature of the sample in a conventional Mössbauer spectral cryostat was controlled with a Lake Shore 332 temperature controller and is accurate to at least 1% of the reported temperatures.

The Mössbauer spectra have been fitted with two Lorentzian doublets that exhibit texture as a result of preferential orientation of the crystallites in the absorber. The texture was treated phenomenologically as the ratio of the area of the low-velocity line to that of the high-velocity line. Statistical fitting errors for the adjusted parameters are given in parentheses throughout the paper. The actual errors are at least two to three times as large.

COMPUTATIONAL METHODS

Nonrelativistic density functional calculations using the *Gaussian09* quantum chemical program[11] have been carried out with the B3LYP functional. Earlier reports[12−14] have indicated that the B3LYP functional is the most reliable for the study of iron(II) complexes. However, a recent paper[10] has reported that the PW91 and BP86 functionals, as well as the B3LYP functional, all provide reasonably good optimized structures for **1** and **2** but that PW91 is best for determining the energy levels. Because of the need to calculate the s-electron density at the iron(II) nucleus, the full 6-311++G(d,p) basis set provided in *Gaussian09* has been used for all atoms and ions in the two complexes. It should be noted that a pseudopotential cannot be used for the iron core electrons in any calculation of the s-electron density at the iron-57 nuclide because the 1s and 2s electrons have a large electron density at the iron-57 nuclide.

Single point electronic energy computations, based on the single crystal X-ray structures, were followed by *Gaussian09* structural optimizations. All computations have been constrained to the sextet state for **1** and quintet state for **2**. The natural orbital populations have been calculated by using the method of Carpenter and Weinhold,[15] and the tensor representation of the electric field gradient has been calculated by the method of Barone.[16] In order to calculate the Mössbauer-effect isomer shift[17] for **2**, single point and optimized computations with the full 6-311++G(d,p) basis set using the *Gaussian09* cubegen full-density option to calculate the core electron density at the manganese and iron nuclei in **1** and **2**.

RESULTS AND DISCUSSION

Mössbauer Spectral Results. The Mössbauer spectra of $[Fe(L_{N4})_2](BF_4)_2$, **2**, have been measured at 4.2, 100, 200, and 295 K and the 4.2 and 200 K spectra[18] are shown in Figure 1; the spectra measured at 100 and 295 K are very similar and all the spectra are shown in Figure S1 in the Supporting Information.

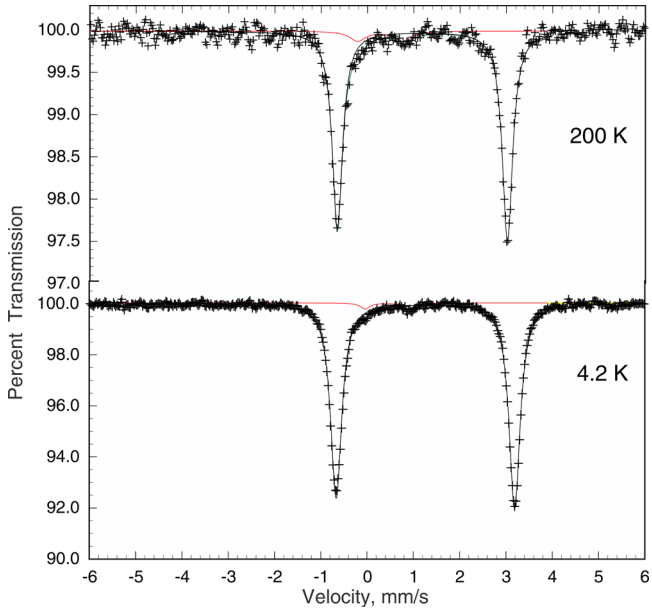

Figure 1. Mössbauer spectra of $[Fe(L_{N4})_2](BF_4)_2$, **2**, measured at 4.2 and 200 K.

The Mössbauer spectra have been fit with two quadrupole doublets, one for the major high-spin iron(II) component in **2** and one for a minor component, an impurity phase most likely arising from traces of iron(III). The resulting fit parameters for the major iron(II) phase are given in Table 1; the parameters for both phases are given in Table S1. Because the spectra clearly show the presence of texture in the absorber resulting from preferential crystallite orientation, the spectra have been fit with a texture parameter that applies to both phases and represents the ratio of the area of the low-velocity line to that of the high-velocity line. Thus, the spectra have been fit with a total of 10 parameters, 2 each for the isomer shift, δ, the quadrupole splitting, ΔE_Q, the line width, Γ, and one each for the texture parameter, the total spectral absorption area, the relative component area, and the baseline. It should be noted that in all the spectra, the preferential crystallite orientation is rather small and corresponds to a ~0.95(1) area ratio between the two components of the major quadrupole doublet observed for **2**.

The isomer shifts, relative to α-iron, observed[19,20] for six-coordinate nitrogen-bonded-iron(II) complexes typically range from 1.00 to 1.10 mm/s at 295 K and from 1.14 to 1.20 mm/s at 4.2 K. Hence, it is apparent in Table 1 that the increase to eight-coordinate iron(II) in $[Fe(L_{N4})_2](BF_4)_2$, **2**, leads, as expected, to somewhat higher isomer shifts, namely, 1.117(4) mm/s at 293 K and 1.260(1) mm/s at 4.2 K. Further, as is shown at the top of Figure 2 the temperature dependence of the isomer shift is normal and may be fit with the Debye model[21,22] for the second-order Doppler shift with a character-

DOI: 10.1021/acs.inorgchem.5b01121
Inorg. Chem. 2015, 54, 8415−8422

Table 1. Observed Mössbauer Spectral Parameters[a] of the Iron(II) in $[Fe(L_{N4})_2](BF_4)_2$, 2

T, K	δ_{Fe}, mm/s[b]	δ_{SNP}, mm/s[c]	ΔE_Q, mm/s	Γ, mm/s	texture[d]	area, %	area, (% ε) (mm/s)
295	1.117(4)	1.382(5)	3.62(1)	0.26(1)	0.90(3)	84(3)	0.97(4)
200	1.184(2)	1.449(3)	3.673(4)	0.272(6)	0.94(2)	93(2)	2.06(4)
100	1.234(4)	1.499(5)	3.81(1)	0.28(2)	0.90(3)	95(2)	5.22(1)
4.2	1.260(1)	1.525(2)	3.854(1)	0.291(2)	0.95(1)	97.6(4)	7.16(4)

[a]Statistical fitting errors are given in parentheses. The actual errors are at least 2–3 times as large. [b]The observed isomer shifts, δ_{Fe}, are reported relative to α-iron foil measured at 295 K. [c]The equivalent isomer shifts, δ_{SNP}, are also given relative to sodium nitroprusside, SNP, by adding 0.2649(8) mm/s to δ_{Fe} [d]The area ratio of the left component of the quadrupole doublet to that of its right component.

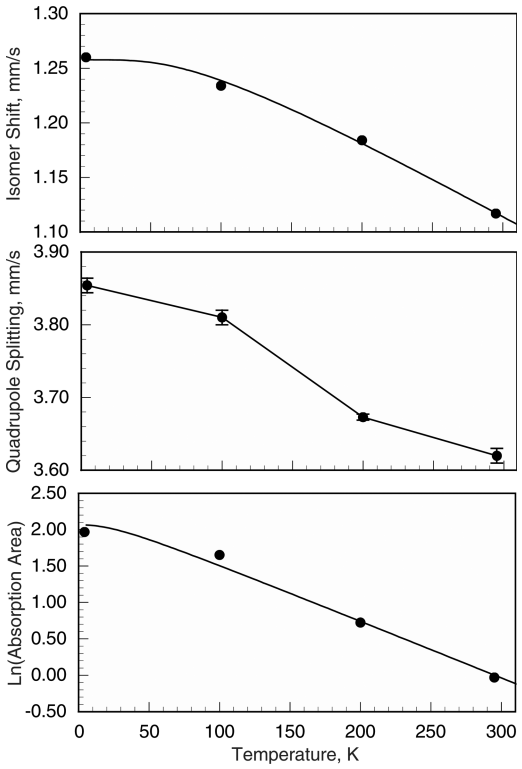

Figure 2. Temperature dependence of the Mössbauer spectral parameters obtained for $[Fe(L_{N4})_2](BF_4)_2$, **2**. The upper and lower solid lines are fits with the Debye model for a solid. The errors are approximately the size of the data points in the upper and lower plots.

istic Mössbauer temperature, Θ_M, of 319(27) K, a value that is typical of high-spin iron(II) complexes.

The temperature dependence of the quadrupole splitting, ΔE_Q, in $[Fe(L_{N4})_2](BF_4)_2$, **2**, is shown in the center of Figure 2. At all temperature ΔE_Q is found to be rather large with a magnitude ranging from 3.854(1) mm/s at 4.2 K to 3.62(1) mm/s at 295 K.

For a high-spin iron(II) complex, there are two contributions to the electric field gradient at the iron-57 nucleus, the valence contribution and the lattice contribution. The former contribution may be substantial if the reduced symmetry at the iron(II) nuclide substantially removes the degeneracy of the t_{2g} and e_g orbitals and leads to very different populations of these orbitals, a population that may be very temperature dependent. The latter contribution, in the absence of significant structural changes upon cooling, typically shows at most small changes with temperature.

Gütlich et al.[23] have reported that a good estimate of the valence contribution, $(\Delta E_Q)_{val}$, to the quadrupole splitting is obtained with a conversion factor of 4.5 mm/s per $(4/7)e\langle r^{-3}\rangle$ obtained from $\langle r^{-3}\rangle = 5a_0^{-3}$, where a_0 is the Bohr radius, and the iron-57 nuclear quadrupole moment, Q, is taken to be 0.16×10^{-28} m^2. Hence, the 6th electron of the iron(II) cation in **2**, an electron which is located[10] in the d_{xy} orbital, will contribute an estimated valence contribution of +4.5 mm/s to the quadrupole splitting. The observed quadrupole splittings of **2** range between 3.854(1) at 4.2 and 3.62(1) mm/s at 295 K. Thus, it appears that the lattice contribution to the quadrupole splitting is negative between 4.2 and 295 K and varies between −0.6 and −0.88 mm/s. This conclusion will be discussed again below in view of the computational results. No viable fit of the temperature dependence of ΔE_Q with the Ingalls[24] model could be obtained, perhaps because a small structural change may occur between 100 and 200 K and yield the decrease of 0.14 mm/s in quadrupole splitting between 100 and 200 K.

For $[Fe(L_{N4})_2](BF_4)_2$, **2**, both the s-electron density at the iron-57 nuclide and the corresponding isomer shift, as well as the electric field gradient at the iron(II) ion, will be discussed below in terms of the density functional calculations.

The temperature dependence of the logarithm of the Mössbauer spectral absorption area is shown at the bottom of Figure 2. Its behavior is normal and may be fit with the Debye model[21,22] with a Debye temperature, Θ_D, of 131(6) K, again a value that is rather typical of high-spin iron(II) complexes. It should be noted that this Θ_D is smaller than the Θ_M of 319(27) K obtained from the temperature dependence of the isomer shift. However, it is well-known[21,22] that Θ_M is typically 2 to 3 times larger than Θ_D because these two temperatures sample different vibrational properties of a lattice. Specifically, the isomer shift depends on $\langle v^2\rangle$, the mean-square vibrational velocity of the iron-57 nuclide and, the absorption area depends on $\langle x^2\rangle$, the mean-square atomic displacement of the iron-57 nuclide; there is no relationship independent model connecting these two mean-square values.[22] Measurements on structurally related six-coordinate molecular iron(II) complexes[21] indicate that Θ_M is often twice the Θ_D value and may be as much as 4 times larger for some high-spin iron(II) salts. It should be noted that this difference is even more pronounced for low-spin iron(II) complexes[21] because the isomer shift depends on $\langle v^2\rangle$, a velocity that is mainly determined by molecular vibrations between 400 and 800 cm^{-1}, whereas the spectral absorption area depends on $\langle x^2\rangle$, a displacement that is mainly determined by the lattice vibrations found below 250 cm^{-1}. Thus, the increase by a factor of ∼2.4 in going from Θ_D to Θ_M in $[Fe(L_{N4})_2](BF_4)_2$, **2**, is characteristic of high-spin iron(II) complexes.

Density Functional Calculations. A summary of the results of the nonrelativistic density functional calculations carried out with the B3LYP functional and the 311++G(d,p) basis set for both the $[Mn(L_{N4})_2]^{2+}$ dication in **1** and $[Mn(L_{N4})_2](ClO_4)_2$, **1**, and both the $[Fe(L_{N4})_2]^{2+}$ dication in **2** and $[Fe(L_{N4})_2](BF_4)_2$, **2**, are summarized in Tables 2–4 for the single-point calculations based on the X-ray structure of

DOI: 10.1021/acs.inorgchem.5b01121
Inorg. Chem. 2015, 54, 8415–8422

Table 2. Calculated Natural Charges and Electronic Configurations

complex	structure	S	electron spin	Mn(II) or Fe(II) charge	electronic configuration[a]
$[Mn(L_{N4})_2]^{2+}$	X-ray[b]	5/2	α	−1.81(3)	$[Ar\alpha]4s^{0.13}3d^{4.85}4p^{0.25}4d^{0.08}$
			β	2.59(3)	$[Ar\beta]4s^{0.12}3d^{0.49}4p^{0.24}4d^{0.06}$
			sum	0.78(3)	$[Ar]4s^{0.25}3d^{5.34}4p^{0.49}4d^{0.14}$
	optimized	5/2	α	−1.77(3)	$[Ar\alpha]4s^{0.13}3d^{4.84}4p^{0.22}4d^{0.07}$
			β	2.68(3)	$[Ar\beta]4s^{0.12}3d^{0.44}4p^{0.22}4d^{0.05}$
			sum	0.91(3)	$[Ar]4s^{0.25}3d^{5.28}4p^{0.44}4d^{0.12}$
$[Mn(L_{N4})_2](ClO_4)_2$, **1**	X-ray[b]	5/2	β	−1.81(3)	$[Ar\alpha]4s^{0.13}3d^{4.85}4p^{0.25}4d^{0.08}$
			β	2.59(3)	$[Ar\beta]4s^{0.12}3d^{0.49}4p^{0.24}4d^{0.06}$
			sum	0.78(3)	$[Ar]4s^{0.25}3d^{5.34}4p^{0.48}4d^{0.14}$
$[Fe(L_{N4})_2]^{2+}$	X-ray[c]	2	α	−1.32(3)	$[Ar\alpha]4s^{0.13}3d^{4.87}4p^{0.26}4d^{0.05}5p^{0.00}$
			β	2.11(3)	$[Ar\beta]4s^{0.13}3d^{1.46}4p^{0.26}4d^{0.04}5p^{0.00}$
			sum	0.79(3)	$[Ar]4s^{0.26}3d^{6.33}4p^{0.51}4d^{0.08}5p^{0.01}$
	optimized	2	α	−1.30(3)	$[Ar\alpha]4s^{0.13}3d^{4.88}4p^{0.23}4d^{0.04}5p^{0.00}$
			β	2.18(3)	$[Ar\beta]4s^{0.13}3d^{1.41}4p^{0.23}4d^{0.03}5p^{0.00}$
			sum	0.89(3)	$[Ar]4s^{0.26}3d^{6.29}4p^{0.46}4d^{0.08}5p^{0.02}$
$[Fe(L_{N4})_2](BF_4)_2$, **2**	X-ray[c]	2	α	−1.32(3)	$[Ar\alpha]4s^{0.14}3d^{4.87}4p^{0.26}4d^{0.05}$
			β	2.120(3)	$[Ar\beta]4s^{0.13}3d^{1.45}4p^{0.26}4d^{0.04}$
			sum	0.80(3)	$[Ar]4s^{0.27}3d^{6.33}4p^{0.52}4d^{0.08}$

[a] $[Ar\alpha]$ corresponds to the nine spin-up α-electrons and $[Ar\beta]$ corresponds to the nine spin-down β-electrons. [b] Structure measured at 293(2) K obtained from ref 1. [c] Structure measured at 293(2) K obtained from ref 2.

Table 3. Calculated Total Energies[a]

complex	structure	energy, Ha	energy, eV	energy, kJ/mol
$[Mn(L_{N4})_2]^{2+}$	X-ray[b]	−3046.255(3)	−82 892.8(1)	−7 997 948(8)
	optimized	−3046.843(3)	−82 908.9(1)	−7 999 494(8)
$[Mn(L_{N4})_2](ClO_4)_2$, **1**	X-ray[b]	−4568.095(3)	−124 304.2(1)	−11 993 542(8)
$[Fe(L_{N4})_2]^{2+}$	X-ray[c]	−3158.942(3)	−85 959.2(1)	−8 293 809(8)
	optimized	−3159.526(3)	−85 975.1(1)	−8 295 343(8)
$[Fe(L_{N4})_2](BF_4)_2$, **2**	X-ray[c]	−4008.4730(3)	−109 076.2(1)	−10 524 254(8)

[a] The calculated energies in Hartrees, Ha, have been converted to eV and kJ/mol with a conversion factor of 27.2114 eV/Ha and 2625.5 (kJ/mol)/Ha, respectively. [b] Structure measured at 293(2) K obtained from ref 1. [c] Structure measured at 293(2) K obtained from ref 2.

Table 4. Calculated HOMO−LUMO Gap Energies[a]

complex	structure	HOMO−LUMO gap (α-spins), eV	HOMO−LUMO gap (β-spins), eV
$[Mn(L_{N4})_2]^{+2}$	X-ray[b]	3.29(16)	3.40(16)
	optimized	3.32(16)	3.21(16)
$[Mn(L_{N4})_2](ClO_4)_2$, **1**	X-ray[b]	1.31(16)	0.22(16)
$[Fe(L_{N4})_2]^{+2}$	X-ray[c]	3.46(16)	2.50(16)
	optimized	3.32(16)	2.67(16)
$[Fe(L_{N4})_2](BF_4)_2$, **2**	X-ray[c]	2.53(16)	2.23(16)

[a] The calculated energies in Hartrees, Ha, have been converted to eV with a conversion factor of 27.2114 eV/Ha. [b] Structure measured at 293(2) K obtained from ref 1. [c] Structure measured at 293(2) K obtained from ref 2.

each moiety. Further, the results for the optimized structures of the $[Mn(L_{N4})_2]^{2+}$ dication in **1** and the $[Fe(L_{N4})_2]^{2+}$ dication in **2** are given in Tables 2−4 and Tables S2 and S3. It should be noted that the $[Fe(L_{N4})_2]^{2+}$ dication in **2** contains 77 atoms or ions and a total of 334 electrons, whereas $[Fe(L_{N4})_2](BF_4)_2$, **2**, contains 87 atoms or ions with 416 electrons. As a consequence of these counts and the extended basis set used, the single point and the optimized calculations on the $[Fe(L_{N4})_2]^{2+}$ dication required 65 and 420 h, respectively, to reach convergence on a numerically intensive computer using six parallel processors.

All of the density functional calculations ignored the solvation molecules present in the X-ray structures of **1** and **2**. Even in the absence of these solvation molecules the actual point group symmetry of the $[Mn(L_{N4})_2]^{2+}$ and $[Fe(L_{N4})_2]^{2+}$ dications is C_1, mainly because of the substantial nonplanarity of both of the L_{N4} ligands. This nonplanarity probably results from the presence of the two anions and the solvation molecules present, a presence that is, of course, reflected in the X-ray structure used in the single point calculations. In contrast, after optimization of the structure of the $[Fe(L_{N4})_2]^{2+}$ dication, its symmetry is essentially S_4; the only deviation from S_4 symmetry arises from a very small, just detectable, "cup-like" nonplanarity of both ligands. Further, upon optimization the four different Fe−N_{imid} bond distances in the $[Fe(L_{N4})_2]^{2+}$ structure in **2** increase from an average bond distance of 2.253(2) Å to four equivalent 2.301(2) Å bond distances, an increase of +0.048(4) Å or 2.1% and the four different Fe−N_{imine} bonds increase from an average of 2.432(2) Å to four equivalent 2.487(2) Å bond distances, an increase of +0.055(4) Å or 2.3%, see Table S3. For comparison, after optimization of the structure of the $[Mn(L_{N4})_2]^{2+}$ dication, its symmetry is extremely close to D_{2d} with no visual deviation from this symmetry. Upon optimization, the four different Mn−N_{imid} bond distances in the $[Mn(L_{N4})_2]^{2+}$ structure in **1** increase from an average bond distance of 2.316(3) Å to four equivalent 2.350(3) Å bond distances, an increase of +0.034(6) Å or 1.5% and the four different Mn−N_{imine} bonds increase from an average of 2.486(3) Å to four equivalent 2.565(3) Å bond distances, an increase of +0.079(6) Å or 3.2%. The iron(II) to

DOI: 10.1021/acs.inorgchem.5b01121
Inorg. Chem. 2015, 54, 8415−8422

Table 5. Calculated and Observed Electric Field Gradients at the Divalent Metal Cations

		calcd				observed	
complex	structure	V_{zz}, a.u.[a]	$eQV_{zz}/2$, mm/s[b]	η	ΔE_Q, mm/s	ΔE_Q, mm/s	T, K
$[Mn(L_{N4})_2]^{2+}$	X-ray[c]	0.114(3)		0.848(1)			
	optimized	−0.202(3)		0.000(1)			
$[Mn(L_{N4})_2](ClO_4)_2$, **1**	X-ray[c]	0.095(3)		0.617(1)			
$[Fe(L_{N4})_2]^{2+}$	X-ray[d]	−2.267(3)	3.666(5)	0.148(1)	3.679(5)		
	optimized	−2.397(3)	3.876(5)	0.000(5)	3.876(5)		
$[Fe(L_{N4})_2](BF_4)_2$, **2**	X-ray[d]	−2.245(3)	3.630(5)	0.144(1)	3.643(5)	3.62(1)	295(2)
						3.854(1)	4.2

[a] 1 au is 9.717×10^{21} V/m^2 and corresponds to $(eQV_{zz})/2$ of 1.617(100) mm/s if the nuclear quadrupole moment is $0.16(1) \times 10^{-28}$ m^2. [b] The numerical accuracy is determined by the numerical accuracy of 3×10^{-3} Ha. If the error in the value of the nuclear quadrupole moment is included the error would be ±0.20 mm/s. [c] Structure measured at 293(2) K obtained from ref 1. [d] Structure measured at 293(2) K obtained from ref 2.

coordinated nitrogen bond distances are all smaller than the analogous bond distances in the manganese(II) complex because of the smaller divalent radius of the iron(II) ion.

The increases in the bond distances upon optimization result from the removal of the "so-called" lattice pressure in calculations that involve only an isolated $[Mn(L_{N4})_2]^{2+}$ or $[Fe(L_{N4})_2]^{2+}$ cation. The resulting optimized bond distances are the same within computational error as those obtained[10] earlier with the B3LYP functional and the TZP, polarized triple-ζ Slater-type orbital basis set.

In Table 2 it is apparent that the calculated natural charges and electronic configurations[15] of both the dication and the full complex of both **1** and **2** are, as expected, very similar. This indicates that the presence of the two anions in the complexes has relatively little effect upon the electronic properties of the eight-coordinate metal(II) cations. In the electronic configurations given in this table, [Arα] corresponds to the nine spin-up α-electrons and [Arβ] corresponds to the nine spin-down β-electrons.

Density Functional Calculation of the Electric Field Gradient. The electric field gradient in atomic units calculated by *Gaussian 09* at the manganese(II) dication, $[Mn(L_{N4})_2]^{2+}$, found in **1**, and the iron(II) dication, $[Fe(L_{N4})_2]^{2+}$, found in **2**, are given in Table 5. From these results it is clear that the inclusion of the two anions decreases by ∼0.02 au, the absolute value of the electric field gradient. In the case of the iron(II) cation, this decrease corresponds to a decrease of 0.03 mm/s in $eQV_{zz}/2$ and ΔE_Q, a decrease that is ∼6 times the numerical accuracy of the calculation or 3 times the experimental accuracy. Thus, this small decrease will not be discussed any further herein, but rather the discussion will concentrate on $[Mn(L_{N4})_2]^{2+}$ and $[Fe(L_{N4})_2]^{2+}$.

Because the manganese(II) cation has a half-filled set of 3d-orbitals, the only contribution to the electric field gradient of +0.114(3) au is a lattice contribution. In contrast, because the iron(II) cation has one additional electron in the d_{xy} orbital,[10] there are two contributions to the calculated electric field gradient of −2.267(3) au, a lattice and a valence contribution. If the lattice contribution is assumed to be similar to that calculated in $[Mn(L_{N4})_2]^{2+}$, then we can conclude that the two contributions are opposite in sign, as is usually observed[24] and as was indicated above. Because the electron charge is negative, the sign of the calculated electric field gradient has to be changed to obtain $eQV_{zz}/2$ and then the quadrupole splitting, ΔE_Q. Thus, the calculated quadrupole splittings in $[Fe(L_{N4})_2]^{2+}$ and **2** are positive in agreement with the positive maximum valence contribution[23] of ∼+ 4.5 mm/s for one electron in the d_{xy} orbital.[10] Further, the calculated values of the quadrupole splitting are in good agreement with the observed values at 4.2 and 295 K, see Table 5.

Upon optimization of the structure of the manganese(II) cation in compound **1**, the parameter η is calculated to be zero, as is expected for the D_{2d}, or essentially S_4, optimized geometry. Because of the change in sign in going from V_{zz} to $eQV_{zz}/2$, the "lattice" contribution increases from −0.114 to +0.202 au, i.e., an increase of 0.316 au upon optimization. If this "lattice" contribution to $eQV_{zz}/2$ is assumed to be similar in the iron(II) cation of compound **2**, an increase of 0.511 mm/s is expected upon optimization, whereas an increase of 0.210 mm/s is calculated and an increase of 0.234 mm/s is observed between 295 and 4.2 K, see Table 5. This increase may be understood as an increase in the negative lattice contribution as a result of a decrease in the "so-called" lattice pressure in a calculation that involves only an isolated cation. In other words a less negative lattice contribution is added to the positive valence contribution and a resulting more positive total quadrupole splitting is calculated. As would be expected for the optimized S_4 symmetry of the structure of the dication in **2**, its asymmetry parameter, η, is 0.00009, a value that is zero within the accuracy of its computation given as 0.000(5) found in Table 5.

In conclusion, the density functional calculation reproduces rather well the observed Mössbauer-effect quadrupole splitting and indicates that, although the value is somewhat larger than is often observed in high-spin iron(II) complexes, it is fully consistent with the expected electronic environment of the eight-coordinate complex.

Density Functional Calculation of the *s*-Electron Probability Density. The Mössbauer spectral isomer shift yields a measure of the *s*-electron probability density at the iron-57 nuclide relative to that found in α-iron, the typical reference material for the iron-57 isomer shift. This *s*-electron probability density is influenced both by the *n*s-orbital populations and by the shielding of this probability density by the 3d electrons found between the nuclide and its 3s and 4s electrons.

The isomer shifts of high-spin iron(II) complexes are in the range of ∼0.7−1.2 mm/s, values that are sensitive to both temperature and the coordination number of the iron(II) ion; in general, the higher the coordination number the higher the isomer shift and, thus the lower the *n*s-electron probability density at the iron-57 nuclide.

Because it is very difficult to carry out *Gaussian09* density functional calculations on an extended array solid such as α-iron, herein the *n*s-electron density is related to that of sodium nitroprusside, SNP, an alternative standard reference material for the iron-57 isomer shift and a molecule for which density

DOI: 10.1021/acs.inorgchem.5b01121
Inorg. Chem. 2015, 54, 8415−8422

Table 6. Calculated s-Electron Density at the Manganese and Iron Nuclides[a]

complex	structure	$\rho(0)$, a_0^{-3}	δ_{SNP}, mm/s calculated	δ_{SNP}, mm/s observed at 295 K	δ_{SNP}, mm/s observed at 4.2 K
$[Mn(L_{N4})_2]^{2+}$	X-ray[b]	10 314.692(5)			
	optimized	10 314.623(5)			
$[Mn(L_{N4})_2](ClO_4)_2$, **1**	X-ray[b]	10 314.688(5)			
$[Fe(L_{N4})_2]^{2+}$	X-ray[c]	11 614.210(5)	1.30(3)		
	optimized	11 614.052(5)	1.35(3)		
$[Fe(L_{N4})_2](BF_4)_2$, **2**	X-ray[c]	11 614.225(5)	1.29(3)	1.382(5)	1.525(2)

[a]All the $\rho(0)$ values were obtained by using the 6-311++G(d,p) basis set for all the structural constituents including the iron(II) and manganese(II) cations. [b]Structure measured at 293(2) K obtained from ref 1. [c]Structure measured at 293(2) K obtained from ref 2.

functional calculation may be carried out by using exactly the same functional and basis set as has been used for the calculations of a given complex, in this case $[Fe(L_{N4})_2](BF_4)_2$, **2**.

The electron probability density, $\rho(0)$, at the iron-57 nucleus in **2** and, for comparison, at the manganese nucleus in **1**, has been calculated from the *Gaussian09* calculated electron probability density; the results are given in Table 6. A pseudopotential cannot be used to calculate $\rho(0)$ and, as a consequence, the $\rho(0)$ values reported in this table and Figure 3 have been calculated by using the 6-311++G(d,p) basis set for all the atoms as well as the iron(II) and manganese(II) ions in **1** and **2**. In both cases the single crystal X-ray structures were used for an initial single point calculation and the starting point for the optimized structure of the dication in **2**. As is shown in Table S3, all the divalent metal to nitrogen distances increase upon optimization and, thus, the decrease in s-electron density at the nucleus, $\rho(0)$, upon optimization is quite normal and expected. Further, the change in $\rho(0)$ in going from **1** to **2** is in the direction expected for the electronic changes, i.e., the ionic radii, the electronegativities, the screening by the 3d-electrons, and the electron affinities, in going from Mn(II) to Fe(II).

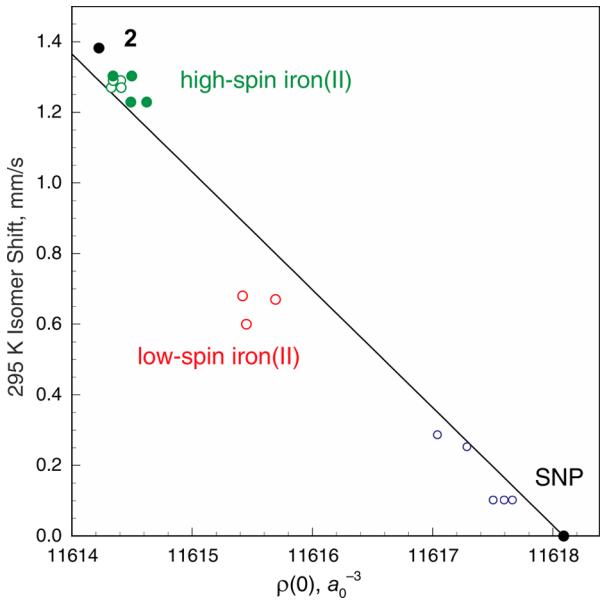

Figure 3. Dependence of the iron-57 isomer shift upon the electron density at the nucleus. The black point corresponds to the high-spin iron(II) in $[Fe(L_{N4})_2](BF_4)_2$, **2**, and the blue points correspond to results for $Fe(CO)_5$ and $Fe_3(CO)_{12}$. The linear fit is anchored to the value obtained for sodium nitroprusside, SNP. The compounds corresponding to the red, green, and blue points are given in refs 25−27.

The correlation between the 295 K observed isomer shift, relative to sodium nitroprusside, in $[Fe(L_{N4})_2](BF_4)_2$, **2**, and the calculated $\rho(0)$ values for a series of related iron complexes[25−27] is shown in Figure 3 in which it is clear that two clusters of points are observed. The first cluster with the high isomer shifts and low $\rho(0)$ values corresponds to the high-spin iron(II) complexes and the second cluster with lower isomer shifts and higher $\rho(0)$ values corresponds to the low-spin iron(II) complexes. The solid line,

$$\delta_{SNP} = -0.334(9)[\rho(0) - 11618.0896] \quad (1)$$

in Figure 3, where δ_{SNP} is in mm/s and $\rho(0)$ is in a_0^{-3}, is the result of a linear least-squares fit that is anchored to the defined zero isomer shift of sodium nitroprusside with $\rho(0)$ = 11618.0896 a_0^{-3}, a value that is calculated for the 295 K X-ray structure of sodium nitroprusside[28] and, in this treatment, is considered an exact number. The residual r^2 value for this fit is 0.97. The identity of the remaining points in Figure 3 may be found in earlier papers.[25,26] The above equation is slightly different from that reported earlier[26] because it uses as an anchor of the linear fit the $\rho(0)$ of sodium nitroprusside. The ±0.03 mm/s accuracy of the calculated isomer shifts given in Table 6 is the result of the ±0.009 a_0^3(mm/s) accuracy of the −0.334(9) a_0^3(mm/s) proportionality constant and not the computational accuracy of $\rho(0)$, which is estimated to be ±0.005 a_0^{-3}.

For the past 10 years, many studies[12−16,29−35] have concentrated on the so-called calibration of the density functional calculations for the prediction of the iron-57 isomer shift in various compounds. Figure 3 is an example of such a calibration and the calibration constant is −0.334(9) a_0^3(mm/s). The good linear correlation observed in Figure 3 was also reported[12−16,29−36] in many of the earlier studies with various functionals and basis sets but the exact value of the calibration constant was found to depend on the choice of the functional and the basis set. For relativistic and nonrelativistic density functional calculations, the calibration constants vary[30−36] from −0.260 to −0.431 a_0^3(mm/s).

However, an alternate, rather different, approach has been reported[37] by Ladrière et al. A radioactive nuclide with an excess of positive nuclear charge may undergo *K*-electron capture decay in order to reduce its charge while maintaining essentially the same nuclide mass.[38] Indeed, the radioactive iron-52 nuclide undergoes a transition to manganese-52 by electron capture with a half-life of 8.3 h and a decay constant that is proportional to the s-electron density present at the surface of the nuclide. By studying several different iron containing compounds made with radioactive iron-52 and comparing their electron capture decay rates with the iron-57 Mössbauer-effect derived isomer shifts, these authors obtained a

DOI: 10.1021/acs.inorgchem.5b01121
Inorg. Chem. 2015, 54, 8415−8422

proportionality constant between the isomer shift and s-electron density of −0.31(4) a_0^3(mm/s).[37]

Recent relativistic calculations yield[35] a calibration constant of −0.294 a_0^3(mm/s), a value that is closer to the experimental value than the earlier nonrelativistic calculations. If the experimental calibration constant[37] of −0.31(4) a_0^3(mm/s) is taken as the most valid value, then the calibration constant of −0.294 a_0^3(mm/s) obtained from relativistic calculations and the calibration constant of −0.334(9) a_0^3(mm/s) obtained herein from nonrelativistic calculations bracket the experimental value of −0.31(4) a_0^3(mm/s) and reside within the rather large uncertainty of this value. Hence, on the basis of these three values, we believe it is not possible, at least for this iron(II) complex, to give a preference to either relativistic or nonrelativistic calculations.

CONCLUSIONS

The iron-57 Mössbauer spectral properties of the eight-coordinate complex, $[Fe(L_{N4})_2](BF_4)_2$, **2**, measured between 4.2 and 295 K are fully consistent with its eight-coordinate structure. As expected the observed isomer shift is somewhat higher than observed for six-coordinate iron(II) complexes but is essentially what one would expect with the increasing coordination number for four, five, and six coordinate complexes with bonding to the nitrogen Lewis-base donor atoms. The temperature dependence of the isomer shift yields a Mössbauer temperature, Θ_M, of 319(27) K. Further, the large quadrupole splitting reflects the very different iron(II) to nitrogen average bond distance of 2.253(2) Å to the imidazole nitrogen donors as compared with the average bond distance of 2.432(2) Å to the benzenediimine nitrogen donors, a difference that yields a large electric field gradient at the iron nucleus and the large quadrupole splitting of 3.854(2) mm/s at 4.2 K.

Density functional calculations with the B3LYP functional and the 6-311++G(d,p) basis set are successful in yielding both an electric field gradient that is in excellent agreement with the observed quadrupole splitting and an s-electron probability density at the iron-57 nuclide that is in good agreement with the observed isomer shift. The analogous calculation of the electric field gradient at the manganese nuclide in $[Mn(L_{N4})_2](ClO_4)_2$, **1**, leads to a small electric field gradient as would be expected in the absence of any valence contribution to the gradient. Upon structural optimization, the coordination environments of both $[Mn(L_{N4})_2]^{2+}$ and $[Fe(L_{N4})_2]^{2+}$ become more symmetric and the bond distances of the divalent cation to the coordinated nitrogen donors increase.

ASSOCIATED CONTENT

Supporting Information

The Supporting Information is available free of charge on the ACS Publications website at DOI: 10.1021/acs.inorgchem.5b01121.

Observed Mössbauer spectral parameters of $[Fe(L_{N4})_2](BF_4)_2$, **2**; calculated natural charges and electronic configurations; X-ray and optimized molecular structure bond distances; and 4.2 to 300 K Mössbauer spectra of **2** (PDF)

AUTHOR INFORMATION

Corresponding Author

*E-mail: glong@mst.edu.

Notes

The authors declare no competing financial interest.

ACKNOWLEDGMENTS

The authors thank Dr. Richard Dawes of the Missouri University of Science and Technology for his assistance with the *Gaussian09* calculations.

REFERENCES

(1) Dube, K. S.; Harrop, T. C. *Dalton Trans.* **2011**, *40*, 7496−7498.
(2) Patra, A. K.; Dube, K. S.; Papaefthymiou, G. C.; Conradie, J.; Ghosh, A.; Harrop, T. C. *Inorg. Chem.* **2010**, *49*, 2032−2034.
(3) King, T. J.; Logan, N.; Morris, A.; Wallwork, S. C. *J. Chem. Soc. D* **1971**, 554−556.
(4) Meier, K.; Rihs, G. *Angew. Chem., Int. Ed. Engl.* **1985**, *24*, 858−859.
(5) Clearfield, A.; Singh, P.; Bernal, I. *J. Chem. Soc. D* **1970**, 389−390.
(6) Di Vaira, M.; Mani, F.; Stoppioni, P. *J. Chem. Soc., Dalton Trans.* **1992**, 1127−1130.
(7) Koch, W. O.; Barbieri, A.; Grodzicki, M.; Schünemann, V.; Trautwein, A. X.; Krüger, H.-J. *Angew. Chem., Int. Ed. Engl.* **1996**, *35*, 422−424.
(8) Diebold, A.; Hagen, K. *Inorg. Chem.* **1998**, *37*, 215−223.
(9) Bu, X.-H.; Lu, S.-L.; Zhang, R.-H.; Liu, H.; Zhu, H.-P.; Liu, Q.-T. *Polyhedron* **2000**, *19*, 431−435.
(10) Conradie, J.; Patra, A. K.; Harrop, T. C.; Ghosh, A. *Inorg. Chem.* **2015**, *54*, 1375−1382.
(11) Frisch, M. J.; Trucks, G. W.; Schlegel, H. B.; Scuseria, G. E.; Robb, M. A.; Cheeseman, J. R.; Scalmani, G.; Barone, V.; Mennucci, B.; Petersson, G. A.; Nakatsuji, H.; Caricato, M.; Li, X.; Hratchian, H. P.; Izmaylov, A. F.; Bloino, J.; Zheng, G.; Sonnenberg, J. L.; Hada, M.; Ehara, M.; Toyota, K.; Fukuda, R.; Hasegawa, J.; Ishida, M.; Nakajima, T.; Honda, Y.; Kitao, O.; Nakai, H.; Vreven, T.; Montgomery, J. A., Jr.; Peralta, J. E.; Ogliaro, F.; Bearpark, M.; Heyd, J. J.; Brothers, E.; Kudin, K. N.; Staroverov, V. N.; Kobayashi, R.; Normand, J.; Raghavachari, K.; Rendell, A.; Burant, J. C.; Iyengar, S. S.; Tomasi, J.; Cossi, M.; Rega, N.; Millam, J. M.; Klene, M.; Knox, J. E.; Cross, J. B.; Bakken, V.; Adamo, C.; Jaramillo, J.; Gomperts, R.; Stratmann, R. E.; Yazyev, O.; Austin, A. J.; Cammi, R.; Pomelli, C.; Ochterski, J. W.; Martin, R. L.; Morokuma, K.; Zakrzewski, V. G.; Voth, G. A.; Salvador, P.; Dannenberg, J. J.; Dapprich, S.; Daniels, A. D.; Farkas, Ö.; Foresman, J. B.; Ortiz, J. V.; Cioslowski, J.; Fox, D. J. *Gaussian 09*, Revision D.01; Gaussian, Inc.: Wallingford, CT, 2009.
(12) Havlin, R. H.; Godbout, N.; Salzmann, R.; Wojdelski, M.; Arnold, W.; Schultz, C. E.; Oldfield, E. *J. Am. Chem. Soc.* **1998**, *120*, 3144−3151.
(13) Godbout, N.; Havlin, R.; Salzmann, R.; Debrunner, P. G.; Oldfield, E. *J. Phys. Chem. A* **1998**, *102*, 2342−2350.
(14) Zhang, Y.; Oldfield, E. *J. Phys. Chem. A* **2003**, *107*, 4147−4150.
(15) Carpenter, J. E.; Weinhold, F. *J. Mol. Struct.: THEOCHEM* **1988**, *169*, 41−62.
(16) Barone, V. *Chem. Phys. Lett.* **1996**, *262*, 201−206.
(17) Gütlich, P.; Bill, E.; Trautwein, A. X. *Mössbauer Spectroscopy and Transition Metal Chemistry, Fundamentals and Applications*; Springer: Heidelberg, Germany, 2011; pp 79−80.
(18) The 4.2 K isomer shift of 1.56 mm/s reported for $[Fe(L_{N4})_2](BF_4)_2$, **2**, in ref 2 is in error. The correct value is δ_{Fe} = 1.260(1) mm/s where the δ_{Fe} value is given relative to α-iron foil at 295 K.
(19) Little, B. F.; Long, G. J. *Inorg. Chem.* **1978**, *17*, 3401−3413.
(20) Reiff, W. M.; Long, G. J. *Mössbauer Spectroscopy Applied to Inorganic Chemistry*; Long, G. J., Ed.; Plenum Press: New York, 1984; Vol. *1*, pp 245−285.
(21) Owen, T.; Grandjean, F.; Long, G. J.; Domasevitch, K. V.; Gerasimchuk, N. *Inorg. Chem.* **2008**, *47*, 8704−8713.
(22) Shenoy, G. K.; Wagner, F. E.; Kalvius, G. M. *Mössbauer Isomer Shifts*; Shenoy, G. K., Wagner, F. E., Eds.; North-Holland: Amsterdam, the Netherlands, 1978; p 49.

DOI: 10.1021/acs.inorgchem.5b01121
Inorg. Chem. 2015, 54, 8415−8422

(23) Gütlich, P.; Bill, E.; Trautwein, A. X. *Mössbauer Spectroscopy and Transition Metal Chemistry, Fundamentals and Applications*; Springer: Heidelberg, Germany, 2011; p 99.
(24) Ingalls, R. *Phys. Rev.* **1964**, *133*, A787−A795.
(25) Remacle, F.; Grandjean, F.; Long, G. J. *Inorg. Chem.* **2008**, *47*, 4005−4014.
(26) Long, G. J.; Tanase, S.; Remacle, F.; Periyasamy, G.; Grandjean, F. *Inorg. Chem.* **2009**, *48*, 8173−8179.
(27) Grandjean, F.; Long, G. J.; Benson, C. G.; Russo, U. *Inorg. Chem.* **1988**, *27*, 1524−1529.
(28) Manoharan, P. T.; Hamilton, W. C. *Inorg. Chem.* **1963**, *2*, 1043−1047.
(29) Neese, F. *Inorg. Chim. Acta* **2002**, *337*, 181−192.
(30) Römelt, M.; Ye, S.; Neese, F. *Inorg. Chem.* **2009**, *48*, 784−786.
(31) Hopmann, K. H.; Ghosh, A.; Noodleman, L. *Inorg. Chem.* **2009**, *48*, 9155−9165; **2011**, *50*, 4221−4221.
(32) Kurian, R.; Filatov, M. *Phys. Chem. Chem. Phys.* **2010**, *12*, 2758−2762.
(33) Sandala, G. M.; Hopmann, K. H.; Ghosh, A.; Noodleman, L. *J. Chem. Theory Comput.* **2011**, *7*, 3232−3247.
(34) Pápai, M.; Vankó, G. *J. Chem. Theory Comput.* **2013**, *9*, 5004−5020.
(35) Hedegård, E. D.; Knecht, S.; Ryde, U.; Kongsted, J.; Saue, T. *Phys. Chem. Chem. Phys.* **2014**, *16*, 4853−4863.
(36) Neese, F.; Petrenko, T. *Mössbauer Spectroscopy and Transition Metal Chemistry, Fundamentals and Applications*; Gütlich, P., Bill, E., Trautwein, A. X., Eds.; Springer: Heidelberg, Germany, 2011; pp 137−199.
(37) Ladrière, J.; Meykens, R.; Coussement, R.; Cogneau, M.; Boge, M.; Auric, P.; Bouchez, R.; Benabed, A.; Godard, J. *J. Phys., Coll. C2* **1979**, *40*, 20−23.
(38) Fridlander, G.; Kennedy, J. W.; Miller, J. M. *Nuclear and Radiochemistry*, 2nd ed.; Wiley: New York, 1964.

DOI: 10.1021/acs.inorgchem.5b01121
Inorg. Chem. 2015, 54, 8415−8422